The *TCF4* Gene Regulates Apoptosis of Corneal Endothelial Cells in Fuchs Endothelial Corneal Dystrophy

Tatsuya Nakagawa,[1] Tetsuro Honda,[1] Taichi Yuasa,[1] Go Nishiuchi,[1] Masakazu Sato,[1] Ayumi Tokunaga,[1] Makiko Nakahara,[1] Theofilos Tourtas,[2] Ursula Schlötzer-Schrehardt,[2] Friedrich Kruse,[2] Prema Padmanabhan,[3] Amit Chatterjee,[4] Gajanan Sathe,[5] Vivek Ghose,[5,6] Narayanan Janakiraman,[4] Derek J. Blake,[7] Noriko Koizumi,[1] Sailaja Elchuri,[4] and Naoki Okumura[1]

[1]Department of Biomedical Engineering, Faculty of Life and Medical Sciences, Doshisha University, Kyotanabe, Japan
[2]Department of Ophthalmology, University of Erlangen-Nürnberg, Erlangen, Germany
[3]Department of Cornea and Refractive Surgery, Sankara Nethralaya, Chennai, India
[4]Department of Nanobiotechnology, Vision Research Foundation, Sankara Nethralaya Campus, Chennai, India
[5]Institute of Bioinformatics, Bangalore, India
[6]Manipal Academy of Higher Education, Manipal, India
[7]Centre for Neuropsychiatric Genetics and Genomics, Division of Psychological Medicine and Clinical Neurosciences, School of Medicine, Cardiff University, Cardiff, United Kingdom

Correspondence: Sailaja Elchuri, Department of Nanobiotechnology, Vision Research Foundation, Sankara Nethralaya, 18 College Rd., Chennai, TamilNadu 600006, India; sailaja.elchuri@gmail.com.
Naoki Okumura, Department of Biomedical Engineering, Faculty of Life and Medical Sciences, Doshisha University, Kyotanabe 610-0394, Japan; nokumura@mail.doshisha.ac.jp.

SE and NO contributed equally to this work and should be considered equivalent authors.

Received: October 24, 2024
Accepted: February 11, 2025
Published: March 6, 2025

Citation: Nakagawa T, Honda T, Yuasa T, et al. The *TCF4* gene regulates apoptosis of corneal endothelial cells in fuchs endothelial corneal dystrophy. *Invest Ophthalmol Vis Sci.* 2025;66(3):16. https://doi.org/10.1167/iovs.66.3.16

Purpose. Fuchs endothelial corneal dystrophy (FECD) is a progressive corneal disorder characterized by excessive extracellular matrix (ECM) accumulation and corneal endothelial cell death. CTG trinucleotide repeat expansion in the transcription factor 4 (*TCF4*) gene represents the most significant genetic risk factor. This study aimed to elucidate the role of *TCF4* in FECD pathogenesis through comprehensive proteomic analysis.

Methods. Corneal endothelial cells isolated from patients with FECD harboring *TCF4* trinucleotide repeat expansion were immortalized to establish an FECD cell model (iFECD). CRISPR/Cas9-mediated genome editing was employed to generate *TCF4*-knockout iFECD cells. Whole-cell proteome analysis was performed using liquid chromatography–mass spectrometry, followed by pathway enrichment analysis of differentially expressed proteins (DEPs). The effects of *TCF4* deletion on TGF-β–mediated protein aggregation and cell death were evaluated using Western blot analysis, flow cytometry, and aggresome detection assays.

Results. Proteomic analysis identified 88 DEPs among 6510 detected proteins. Pathway analysis revealed significant enrichment in ECM-associated pathways, oxidative stress responses, and cellular motility. *TCF4* deletion attenuated TGF-β–induced cell death in iFECD cells. Concordantly, Western blot analysis demonstrated that *TCF4* deletion suppressed TGF-β2–mediated cleavage of caspase-3 and poly (ADP-ribose) polymerase. Flow cytometric analysis of Annexin V–positive cells confirmed reduced apoptosis in *TCF4*-deleted cells following TGF-β2 treatment. Additionally, aggresome detection assays revealed that *TCF4* deletion diminished TGF-β2–induced protein aggregation.

Conclusions. This study demonstrates a crucial role for *TCF4* in FECD pathogenesis, particularly in ECM regulation and protein aggregation–induced cell death.

Keywords: fuchs endothelial corneal dystrophy, corneal endothelial cells, *TCF4*

Fuchs endothelial corneal dystrophy (FECD) is a progressive bilateral disorder characterized by dysfunction and degeneration of the corneal endothelium, with consequent corneal edema and severe vision impairment. The formation of excrescences of the Descemet's membrane (basement membrane) due to excessive extracellular matrix (ECM) production is a clinical hallmark of FECD.[1,2] The prevalence of FECD ranges between 4% and 11%.[3–6] A recent meta-analysis that demonstrated a 7.33% prevalence among 4748 subjects identified FECD as the most common inherited corneal dystrophy.[7] Several genes, including *AGBL1*, *LOXHD1*, *SLC4A11*, and *ZEB1*, have been implicated in late-onset FECD,[8–14] but mutations in these genes are relatively rare.[15] Most FECD cases are associated with a CTG trinucleotide repeat expansion in the *TCF4* gene, which is recognized as the most significant genetic factor.[16–23] This expansion has advanced our understanding of FECD pathophysiology and has implicated several mechanisms, including RNA-mediated toxicity, dysregulated *TCF4* expression, and repeat-associated non-AUG translation.[19,24–29]

The pathogenesis of FECD also involves activated TGF-β signaling and epithelial–mesenchymal transition (EMT).[30–32] However, many aspects of this genetic mutation remain unclear, including how it causes specific cellular impairments and the variability in clinical symptoms.[23]

Several research groups, including ours, have investigated *TCF4* gene expression, isoform variation, and differential exon usage in the corneal endothelium of patients with FECD.[33–39] Indeed, transcriptomics has identified dysregulated expression of *TCF4*, and this dysregulation is proposed as one of the potential pathologic mechanisms underlying FECD.[33–39] However, the influence of *TCF4* on the expression of other molecules, especially at the protein level, has not been comprehensively investigated, largely due to the limited availability of adequate quantities of patient corneal endothelial samples. Proteomics exploration is an essential addition to transcriptome analysis because it examines the actual proteins that are produced, their modifications, and their interactions, which are not reflected at the RNA level.[40–43]

Therefore, in the current study, we utilized an FECD cell model and CRISPR/Cas9 to investigate the comprehensive impact of *TCF4* knockout on the expression of other proteins. We investigated differentially expressed proteins (DEPs) induced by *TCF4* knockout and performed pathway analyses. We also assessed the effect of *TCF4* knockout on TGF-β–mediated unfolded protein deposition and cell death in the FECD cell model.

Materials and Methods

Ethics Statement

The human tissue used in this study was handled under the guidelines of the Declaration of Helsinki. Institutional review board approvals for research involving human subjects were obtained from the Friedrich-Alexander University Erlangen-Nürnberg (Applied number: 140_20 B) and Doshisha University (Applied number: 20009). Informed consent was acquired from patients with FECD who underwent Descemet's membrane endothelial keratoplasty at the Friedrich-Alexander University Erlangen-Nürnber. Patients who were unable to provide informed consent, prisoners, and vulnerable populations were excluded from the study. Additionally, patients with advanced FECD, for whom insufficient corneal endothelial cells could be collected for RNA sequencing analysis, were also excluded. Stripped Descemet's membranes, including corneal endothelial cells, were obtained following the surgery.

Culture of Corneal Endothelial Cells Derived From a Patient With FECD

Immortalized corneal endothelial cells derived from patients with FECD (iFECD) were established previously and used in this study.[30] The iFECD cells were cultured in Dulbecco's Modified Eagle Medium (DMEM; Nacalai Tesque, Kyoto, Japan) containing 10% fetal bovine serum (FBS) and 1% penicillin and streptomycin (Nacalai Tesque). When the cells reached 80% confluency, they were passaged using 0.05% Trypsin-EDTA (Nacalai Tesque). For some experiments, iFECD cells were cultured until 80% confluency and further cultured with fresh DMEM without FBS supplemented with 10 ng/mL TGF-β2 (Wako Pure Chemical Industries, Ltd., Osaka, Japan) for 24 hours.

Knockout of the *TCF4* Gene Using the CRISPR–Cas9 System

The basic helix–loop–helix (bHLH) in *TCF4* of iFECD or 20 bases in exon 9 in *TCF4* of iFECD were knocked out using CRISPR/Cas9 (hereafter, iFECD *TCF4*ΔbHLH, iFECD *TCF4*$^{-/-}$). Guide RNA (gRNA) for CRISPR–Cas9 was designed on Feng Zhang's website (http://crispr.mit.edu/; Massachusetts Institute of Technology; site no longer active). The insert oligonucleotides for bHLH in *TCF4* deletion gRNA-1 were 5′-CACCGCCACAGCAATAATGACGATG-3′ and 5′-AAACCATCGTCATTATTGCTGTGGC-3′, and for bHLH in *TCF4* deletion gRNA-2, they were 5′-CACCGAGT CTGGAGCAGCAAGTCCG-3′ and 5′-AAACCGGACTTGCTG CTCCAGACTC-3′ for the *TCF4* gene (Gene ID: 6925). Insert oligonucleotides for 20 bases in exon 9 in *TCF4* deletion gRNA-1 were 5′-CACCGGACTACAAATAGGGACTCGCC-3′ and 5′- AAACGGCGAGTCCCTATTGTAGTC-3′, and insert oligonucleotides for 20 bases in exon 9 in *TCF4* deletion gRNA-2 were 5′-CACCGCAAGCACTGCCGACTACAAT-3′ and 5′- AAACATTGATGTCGGCAGTGCTTG-3′ for the *TCF4* gene.

The complementary oligonucleotides for gRNA were annealed and cloned into lentiCRISPR v2, gifted from Feng Zhang (Addgene plasmid #52961; http://n2t.net/addgene:52961; RRID:Addgene_52961; Addgene, Watertown, MA, USA). The insertions of the gRNAs were assessed using Sanger sequencing (SeqStudio Gentic Analyzer, Thermo Fisher Scientific, Waltham, MA, USA). Each plasmid vector was cotransfected with psPAX2 (Plasmid #12260; Addgene) and pCMV-VSV-G (Plasmid #8454; Addgene) into 293T cells using OptiMEM-I with Lipofectamine 3000 (Thermo Fisher Scientific). Lentiviral supernatants were harvested after 24 hours and concentrated using Lenti-X Concentrator (Clontech Laboratories, Inc., Mountain View, CA, USA) according to the manufacturer's protocol. iFECD cells were cultured in 6-well plates to ~70% confluency with DMEM supplemented with 10% FBS and penicillin/streptomycin (Nacalai Tesque). Lentiviral concentrates (100 µL), polybrene (5 µg/mL; Nacalai Tesque), and puromycin (1 µg/mL; InvivoGen, San Diego, CA, USA) were added to the culture medium, and iFECD cells were further cultured. After 5 days, the surviving cells were collected and cultured as single cells in 96-well plates to establish single-cell clones. The single-cell clones were isolated and passaged after 14 to 17 days of culture.

Genomic DNA Analysis and Sequencing

Cultured cells were harvested using 0.05% Trypsin-EDTA, centrifuged, and then lysed using a MonoFas gDNA Cultured Cells Extraction Kit VI (Animos, Saitama, Japan) to extract DNA. Forward primer (5′-CTTACTCCTGTTAAGCTGCCTTG -3′) and reverse primer (5′-CTAAATCCATAAGGCAGCATCCC -3′) were used to confirm the deletion of bHLH. The PCR products were amplified using a T3000 thermocycler (Analytik jena, Jena, Germany) under the following conditions: 35 cycles of denaturation at 95°C for 20 seconds, annealing at 55°C for 20 seconds, and elongation at 72°C for 20 seconds. The PCR amplicons were subjected to electrophoretic separation on 1% agarose gels, followed by

Investigative Ophthalmology & Visual Science

staining with ethidium bromide, and visualized under ultraviolet light using an Amersham Imager 600 (GE Healthcare, Chicago, IL, USA). The PCR amplicons were purified using ExoSAP-IT (Thermo Fisher Scientific). The sequence of the treated PCR products was confirmed by Sanger sequencing (SeqStudio Gentic Analyzer, Thermo Fisher Scientific) with the following primers: forward primer (5′-CTTACTCCTGTTAAGCTGCCTTG-3′) and reverse primer (5′-CTAAATCCATAAGGCAGCATCCC-3′) for iFECD *TCF4*ΔbHLH and forward primer (5′- GTAAAACGACGGCCAGT-3′) and reverse primer (5′-CAGGAAACAGCTATGAC-3′) for iFECD *TCF4*$^{-/-}$.

Protein Isolation for Mass Spectrometry

The iFECD and iFECD *TCF4*ΔbHLH cells were washed with PBS, detached using TrypLE (Thermo Fisher Scientific), and washed again three times with PBS. The cell pellets were flash frozen in liquid nitrogen and preserved at −80°C for future analysis. The cell pellets were lysed by sonication in a buffer containing 2% SDS and 50 mM triethylammonium bicarbonate, supplemented with Halt Protease and Phosphatase Inhibitor Cocktail (Thermo Fisher Scientific). After sonication, the lysates were centrifuged, and the supernatant was collected for protein quantification using the BCA protein assay. Protein quality was verified by electrophoresis of 20 µg protein on a 10% SDS-PAGE gel. Reduction and alkylation of proteins were achieved by treating the samples with 5 mM dithiothreitol at 60°C for 1 hour, followed by 10 mM iodoacetamide at room temperature for 30 minutes in the dark. The proteins were precipitated using ice-cold acetone and an incubation period of 12 hours at 4°C, after which the samples were centrifuged, and the resultant pellet was resuspended in 50 mM triethylammonium bicarbonate. This was followed by enzymatic digestion with trypsin (Promega, Madison, WI, USA) for 12 hours. The resulting peptides were purified using a Sep-Pak C_{18} Plus Light Double Luer-Lock Cartridge (Waters, Milford, MA, USA). The digested peptides were acidified with 1% formic acid and centrifuged, and the supernatants were collected. A Sep-Pak column was activated using 100% acetonitrile, followed by 0.1% formic acid, and then acidified peptide samples were loaded onto the column, washed with 0.1% formic acid, and eluted with 40% acetonitrile in 0.1% formic acid. Following elution, the peptides were dried and resolubilized in 100 mM triethylammonium bicarbonate buffer (TEAB) and subsequently labeled with TMT10plex Isobaric Label Reagents and Kits (Thermo Fisher Scientific), following the manufacturer's instructions.

Basic pH Reverse Phase Liquid Chromatography Fractionation

The labeled peptides were solubilized in 1 mL basic pH RPLC solvent A (7 mM TEAB, pH 8.5) and fractionated by basic pH reverse phase liquid chromatography (bRPLC) on an XBridge BEH C_{18} Column (Waters), employing a progressively increasing gradient of bRPLC solvent B (7 mM TEAB, pH 8.5, 90% acetonitrile), utilizing an Agilent 1260 HPLC system (Agilent Technologies, Santa Clara, CA, USA). The flow rate for the mobile phase was set at 0.3 mL/min, and the eluted peptides were monitored by absorbance changes at 280 nm. The procedure was completed over a total duration of 90 minutes, yielding a collected volume of 27 mL. Subsequently, the 96 fractions were consolidated into 12 fractions and vacuum dried.

Liquid Chromatography/Tandem Mass Spectrometry Analysis

Lyophilized peptides were resuspended in 0.1% formic acid and analyzed using an Orbitrap Fusion Lumos Mass Spectrometer (Thermo Fisher Scientific) interfaced with an Easy-nLC 1200 nanoflow liquid chromatography system (Thermo Fisher Scientific). The peptides were applied to a precolumn (nanoViper; 100 µm × 20 mm, Thermo Fisher Scientific) at a flow rate of 3 µL/min for enrichment and subsequently separated on an analytical column (HPLC Column Acclaim RSLC 120 C18, 75 µm × 50 cm; Thermo Fisher Scientific) at a flow rate of 280 nL/min. The elution was performed using a step gradient of 8% to 22% solvent (0.1% formic acid in 95% acetonitrile) over 70 minutes, followed by an increase to 22% to 35% solvent for a duration of 70 to 103 minutes. The total acquisition time was set at 120 minutes. The mass spectrometer was operated in a data-dependent acquisition mode. Survey full-scan mass spectrometry (MS) (from m/z 350–1600) was acquired in the Orbitrap at a resolution of 120,000 at 200 m/z. The AGC target for MS1 was set at 4×10^5 and the ion filling time was set at 50 ms. The most intense ions with charge state ≥2 were isolated with isolation window 1.6 in a 3-second cycle and fragmented using higher-energy collisional dissociation (HCD) fragmentation with 34% normalized collision energy and detected at a mass resolution of 50,000 and an ion injection time of 100 ms.

Analysis of DEPs

For protein identification and quantification, the SEQUEST search algorithm was employed using Proteome Discoverer software against the Human RefSeq protein database. The search parameters included a maximum of two missed cleavages. Carbamidomethylation at cysteine and TMT 10-plex (+229.163) modification at the N-terminus of peptide and lysine were set as fixed modifications, while oxidation of methionine was a variable modification. For MS data, monoisotopic peptide mass tolerance was set to 10 ppm and MS/MS tolerance to 0.1 Da. A false discovery rate of 1% was set at the peptide-spectrum match level as well as at 1% at the protein level.

Subsequent analyses were conducted using Perseus software[44] to compute fold changes and P values through t-tests, with fold changes undergoing logarithmic transformation to the $\log_2$ scale. The criteria for identifying DEPs included thresholds of $|\log_2$ fold changes$|$ (≥0.5) and P values (<0.05). A volcano plot, integrating $\log_2$ fold changes and P values, was generated to depict the distribution of each protein, utilizing the ggplot2 package in R. Proteins upregulated in iFECD *TCF4*ΔbHLH relative to iFECD were marked with red dots, whereas downregulated proteins were denoted with blue dots. Additionally, heatmap clustering was performed using the heatmap.2 function within the gplot package for R, with all protein expression levels normalized to z-scores and illustrated across a spectrum from +2 to −2. Red stripes represented relatively high expressions, and blue stripes indicated relatively low expressions.

Investigative Ophthalmology & Visual Science

Functional Enrichment and Protein–Protein Interaction Analyses

Gene Ontology (GO) analysis[45] was performed using the ClusterProfiler package (version 4.2.2)[46] in R. Significantly enriched GO terms were determined with a P value threshold of <0.05. The top 12 GO terms, representing biological processes (BP), cellular components (CC), and molecular functions (MF), were selected and graphically visualized using the ggplot2 package (version 3.3.6) in R. For pathway-based enrichment analysis, Reactome[47] and Kyoto Encyclopedia of Genes and Genomes (KEGG)[48,49] analyses were also conducted. KEGG pathway analysis was conducted with the ClusterProfiler package and illustrated using the ggplot2 package in R. Reactome pathway analysis was carried out using the ReactomePA (version 1.38.0) and ggplot2 packages. Significantly enriched pathways, identified with a $P <$ 0.05, were visually presented, showcasing the top 12 pathways based on their significant gene ratio on the x-axis. P values were converted with "$-\log_{10}$," then displayed with colors ranging from blue to red using the scales package. For protein–protein interaction (PPI) networks, GeneMANIA (http://genemania.org/), an accessible online tool, was employed.

Confirmation of Altered ECM-Related Molecules at the mRNA Level Using RNA Sequencing Data

Our RNA sequencing (RNA-seq) data for the corneal endothelium derived from patients with FECD and healthy subjects were obtained from the DDBJ database.[38] Two other RNA-seq data sets available at the GEO repository were also downloaded.[50,51] Data preprocessing was conducted utilizing fastp for the removal of adapter bases and low-quality reads.[52] The refined reads were then mapped to the reference genome via the STAR alignment tool, with gene expression quantification achieved through RSEM.[53,54] Differential gene expression analysis was performed employing the DESeq2 package in R, applying criteria for adjusted P values to compare gene expression in the corneal endothelium of patients with FECD against gene expression in healthy controls. The expression levels for specific genes of interest were visualized by constructing boxplots in R utilizing the ggplot2 package.

Immunocytochemistry and Aggresome Staining

Cells were fixed with 4% paraformaldehyde for 10 minutes, permeabilized using 1% Triton X-100 (Nacalai Tesque), and subsequently blocked with 2% bovine serum albumin to prevent nonspecific binding. The samples were incubated overnight at 4°C with primary antibodies against fibronectin (dilution 1:1000; BD Biosciences, Franklin Lakes, NJ, USA). Alexa Fluor 488–conjugated goat anti-mouse antibodies (Life Technologies, Carlsbad, CA, USA) were used as secondary antibodies, applied at a dilution of 1:1000 and incubated at 37°C for 45 minutes. Aggresomes were identified using an aggresome-specific reagent (dilution 1:1000; Enzo Life Science, Farmingdale, NY, USA) at 37°C for 45 minutes. Nuclei were stained with DAPI (Vector Laboratories, Carlsbad, CA, USA). Fluorescence microscopy analysis was conducted using a DM 2500 microscope (Leica Microsystems, Wetzlar, Germany). Colocalization analysis was performed using the ImageJ software (version 1.54f; National Institutes of Health, Bethesda, MD, USA). Manders's coefficients were calculated to quantify the degree of colocalization between aggresome and fibronectin signals.

Western Blotting

The cells from iFECD, iFECD *TCF4*$^{-/-}$, and iFECD *TCF4*ΔbHLH were rinsed with ice-cold PBS and lysed using ice-cold radioimmunoprecipitation assay buffer supplemented with phosphatase inhibitor cocktail 2 (Millipore-Sigma, Burlington, MA, USA) and a protease inhibitor cocktail (Roche Applied Science, Penzberg, Germany). The lysates were centrifuged at 800 × g for 10 minutes, and the concentration of total proteins in the supernatants was determined utilizing the BCA Protein Assay Kit (Thermo Fisher Scientific). The proteins were then separated by SDS-PAGE and transferred onto PVDF membranes, which were then blocked with 3% nonfat dry milk for 1 hour at room temperature and incubated overnight at 4°C with primary antibodies against cleaved caspase-3 (1:1000; Cell Signaling Technology, Danvers, MA, USA), cleaved poly (ADP-ribose) polymerase (cleaved PARP) (1:1000; Cell Signaling Technology), glyceraldehyde-3-phosphate dehydrogenase (GAPDH) (1:3000; Medical & Biological Laboratories Co., Ltd., Tokyo, Japan), TCF4[55] (1:500), Snail1 (1:1000; Cell Signaling Technology), ZEB1 (1:1000; Cell Signaling Technology), fibronectin (1:20,000; BD Biosciences), phosphorylated Smad3 (p-Smad3) (1:1000; Cell Signaling Technology), Smad2 (1:1000; Cell Signaling Technology), phosphorylated Smad2 (p-Smad2) (1:1000; Cell Signaling Technology), and Smad3 (1:1000; Cell Signaling Technology). Following primary antibody incubation, the blots were washed and incubated with horseradish peroxidase–conjugated secondary antibodies (1:5000; GE Healthcare, Chicago, IL, USA) and visualized using luminal-based enhanced chemiluminescence with the ECL Advanced Western Blotting Detection Kit (Nacalai Tesque). The relative density of immunoblot bands from Western blot analyses was quantified using ImageJ software.

Flow Cytometry

For flow cytometry analysis, control and TGF-β2–treated cells were stained with DMEM containing Annexin V (Medical & Biological Laboratories Co., Ltd.) for 15 minutes and harvested using Accumax (Innovative Cell Technologies, San Diego, CA, USA). Flow cytometric analysis was performed using CellQuest Pro software (BD Biosciences) for data acquisition and analysis.

Statistical Analysis

All statistical analyses were performed using R software. For comparisons between two groups, statistical significance was assessed using Student's t-test. For multiple group comparisons, Dunnett's multiple-comparisons test was applied. Statistical significance was defined as $P < 0.05$ for all analyses. Results are presented as mean ± SEM.

Results

Knockout of the bHLH in *TCF4* in an iFECD

In this study, we employed an in vitro model of iFECD due to the limited availability of corneal endothelial cells obtainable from surgical specimens of patients with FECD.

Investigative Ophthalmology & Visual Science

We first generated the *TCF4* knockout iFECD for proteome analysis to evaluate the effect of *TCF4* on other molecules at the protein level. Representative images obtained with phase-contrast microscopy showed that iFECD exhibited a polygonal and monolayer structure. The iFECD *TCF4*ΔbHLH variant with a deletion in the bHLH domain that abrogates *TCF4*'s function as a transcription factor also exhibited a morphology similar to that of the control iFECD (Fig. 1A). The PCR product size of the genomic DNA of the *TCF4* gene was approximately 900 bp in iFECD and 700 bp in iFECD *TCF4*ΔbHLH (Fig. 1B), showing the successful deletion of the bHLH domain. Western blotting showed the successful suppression of TCF4-A (54 kDa) (NM_001243234.2) and TCF4-B (72 kDa) (NM_001083962.2) (Fig. 1C). Quantitative analysis further demonstrated a significant reduction in TCF4-A and TCF4-B expression levels in iFECD *TCF4*ΔbHLH compared to iFECD (Fig. 1D). Sanger sequencing also confirmed the absence of the bHLH domain in the *TCF4* region (Fig. 1E). (Note that the upstream and downstream bases of the bHLH domain are indicated by red or blue lines, respectively.)

Identification of DEPs

DEPs between iFECD and iFECD *TCF4*ΔbHLH were identified using mass spectrometry for quantitative whole-cell proteomics to elucidate the molecular changes induced by *TCF4* functional deletion in corneal endothelial cells derived from patients with FECD. The volcano plot revealed a global overview of the protein expression distributions of iFECD compared to the iFECD *TCF4*ΔbHLH (Fig. 2A). Among a total of 6510 proteins detected, 88 DEPs were found, including 52 upregulated (indicated in red dots) and 36 downregulated proteins (in blue dots) with thresholds of $|\log_2(\text{fold change})| \geq 0.5$ and $P < 0.05$ (Fig. 2A). A heatmap illustrated a hierarchical clustering of the iFECD and iFECD *TCF4*ΔbHLH representing variations in the relative abundance of all detected proteins with row *z*-scores ranging from −2 (blue) to +2 (red). A heatmap showed a visually split hierarchical clustering into two groups consisting of iFECD and iFECD *TCF4*ΔbHLH groups and the similarity within each group (Fig. 2B). The top 30 upregulated and downregulated proteins in iFECD *TCF4*ΔbHLH compared to iFECD are shown in Tables 1 and 2, respectively. The top three upregulated proteins in the iFECD *TCF4*ΔbHLH were alpha-2A adrenergic receptor (ADRA2A), carbonic anhydrase 2 isoform 1 (CA2), and retinal dehydrogenase 1 (ALDH1A1) (Table 1). The top three downregulated proteins were keratin, type I cytoskeletal 19 (KRT19); calponin-1 isoform 1 (CNN1); and contactin-associated protein 1 precursor (CNTNAP1) (Table 2).

Enrichment Analysis of DEPs

GO enrichment analysis was carried out using the 88 DEPs associated with the knockout of *TCF4* (Fig. 3). The GO terms were subdivided into three categories: BP, CC, and MF. Response to oxidative stress, response to toxic substances, and cellular response to chemical stress were significantly enriched in BP. The apical part of the cell, collagen-containing ECM, and cell–cell junction were significantly enriched in CC. Actin binding, ECM structural constituent, and cadherin binding were significantly enriched in MF.

Reactome pathway analysis indicated that DEPs were enriched in the metabolism of carbohydrates, ECM organization, transport of inorganic cations/anions and amino acids/oligopeptides, cell surface interactions at the vascular wall, and collagen formation (Fig. 4A). KEGG pathway analysis demonstrated the enrichment of proteoglycans in cancer, sphingolipid metabolism, protein digestion and absorption, ECM–receptor interaction, and ferroptosis (Fig. 4B).

The proteins altered by the knockout of *TCF4* were further analyzed by creating PPI networks using GeneMANIA. For upregulated proteins, the solute carrier (SLC) protein family strongly interacted in the network, indicating an enrichment of amino acid–associated functions (Supplementary Fig. S1A). For downregulated proteins, ECM-related functions were potentially involved in *TCF4*, as extracellular structure organization and ECM organization were significantly enriched in the network (Supplementary Fig. S1B).

Our enrichment analyses indicated the enrichment of multiple pathways related to ECM; therefore, we also investigated the expression level of the pathway-related mRNA corresponding to the DEPs using previously published RNA-seq data, including our own.[38,50,51] In terms of DEPs related to ECM organization (GO:0030198), *COL1A2*, *COL8A1*, and *SULF1* were downregulated, and *LUM*, *ANTXR1*, *CCN1*, and *NPNT* were upregulated. The mRNA expression levels evaluated by three RNA-seq data sets revealed distinctive patterns of ECM-related molecules in corneal endothelial cells from patients with FECD compared to controls. Three genes showed consistent upregulation across all data sets: *ANTXR1*, *SULF1*, and *COL1A2* (Figs. 5A–C). *FLNB* was upregulated in both Nakagawa et al.[38] and Chu et al.[50] but not in Nikitina et al.[51] (Fig. 5D), while *CCN1* showed increased expression in Nikitina et al.[51] and Chu et al.[50] but not in Nakagawa et al.[38] (Fig. 5E). *SDC1* exhibited opposite expression patterns between data sets: decreased expression in Nakagawa et al.[38] and increased expression in Nikitina et al.[51] with no significant changes in Chu et al.[50] (Fig. 5F). *COL8A1* showed significant upregulation only in Nakagawa et al.[38] (Fig. 5G). In contrast, *LUM* and *HAPLN1* showed no significant changes across all data sets (Figs. 5H, 5I). These results suggest that these pathologic ECM molecules are at least partially regulated by *TCF4*.

Effect of *TCF4* Deletion on TGF-β2–Mediated ECM Production and Apoptosis

We previously reported that the TGF-β signaling pathway plays an important role in producing excessive ECM and subsequent unfolded protein response–mediated apoptosis[56,57]; therefore, we evaluated the effect of *TCF4* deletion using the FECD cell model. For these experiments, in addition to iFECD *TCF4*ΔbHLH (featuring deletion of the bHLH domain in *TCF4*), we utilized iFECD *TCF4*$^{-/-}$ (harboring a 20-base deletion in exon 9 of *TCF4*) to further corroborate the effects of *TCF4* knockout. Phase-contrast images of iFECD, iFECD *TCF4*$^{-/-}$, and iFECD *TCF4*ΔbHLH showed a monolayer sheetlike structure with polygonal cell morphology resembling an in vivo corneal endothelial monolayer (Fig. 6A, left). Consistent with our previous report,[30] the phase-contrast images showed that TGF-β2 induced cell death in iFECD. By contrast, no cell death was induced by TGF-β2 in iFECD *TCF4*$^{-/-}$ and iFECD *TCF4*ΔbHLH (Fig. 6A, right). Sanger sequencing confirmed that 20 bases in exon 9 in *TCF4* were deleted in iFECD *TCF4*$^{-/-}$ (note that the 20 bases in exon 9 in *TCF4* are indicated by red lines) (Fig. 6B). The exon numbers refer to TCF4-B (NM_001083962.2). West-

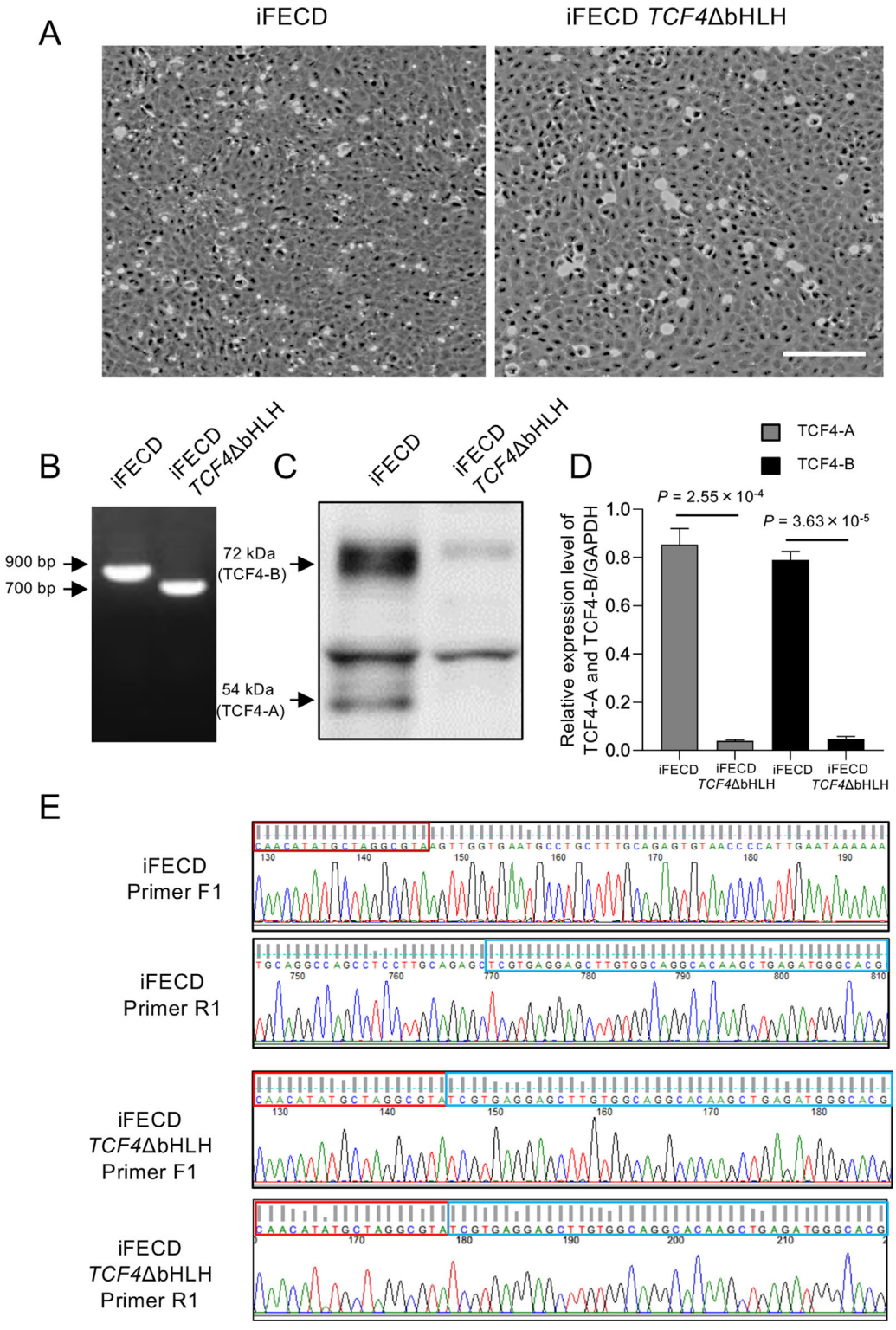

Figure 1. Knockout of the bHLH in *TCF4* in the FECD cell model (iFECD). (**A**) iFECD cells were established from patient-derived corneal endothelial cells. Using CRISPR/Cas9, either the bHLH region or 20 bases in exon 9 of *TCF4* were knocked out (iFECD *TCF4*ΔbHLH, iFECD *TCF4*$^{-/-}$). Phase-contrast microscopy images show that iFECD retains a polygonal, monolayer structure, similar to iFECD *TCF4*ΔbHLH. *Scale bar*: 200 µm. (**B**) PCR analysis showed genomic DNA product sizes of approximately 900 bp in iFECD and 700 bp in iFECD *TCF4*ΔbHLH. Experiments were repeated independently at least three times with consistent results; representative images are shown. (**C**) Western blotting confirmed the suppression of TCF4-A (54 kDa, NM_001243234.2) and TCF4-B (72 kDa, NM_001083962.2). Experiments were conducted in three independent replicates with reproducible results. (**D**) Densitometric analysis of TCF4 protein expression levels. Values were normalized to GAPDH and are expressed as mean ± SEM from three independent experiments. (**E**) Sanger sequencing verified the absence of the bHLH domain in the *TCF4* region. *Red* and *blue lines* indicate bases upstream and downstream of the bHLH domain, respectively.

Investigative Ophthalmology & Visual Science

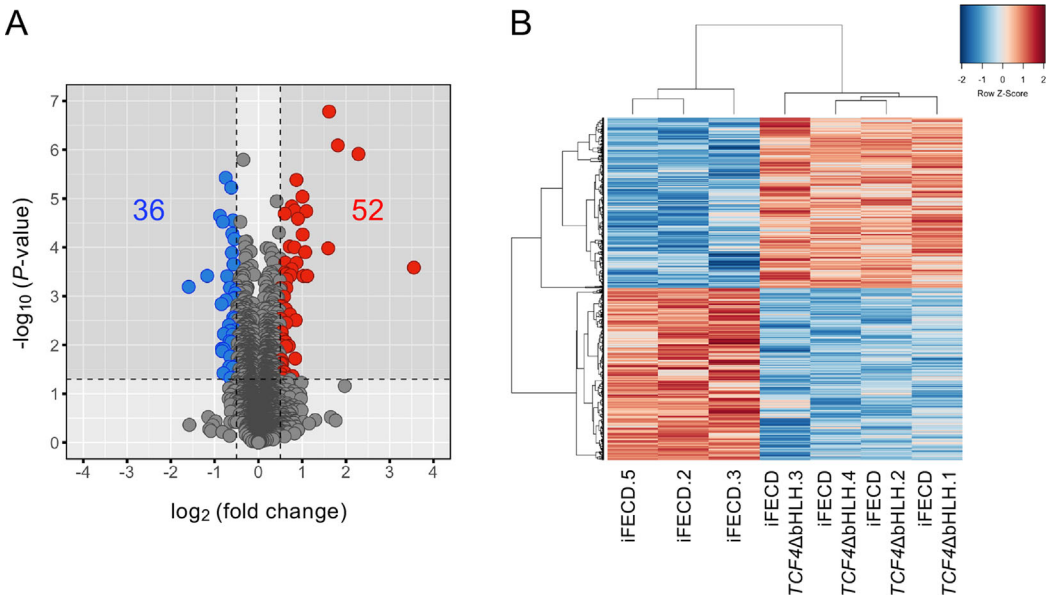

Figure 2. Identification of DEPs between FECD cell model (iFECD) and iFECD *TCF4*ΔbHLH. (**A**) The volcano plot provides an overview of protein expression in iFECD compared to iFECD *TCF4*ΔbHLH. Mass spectrometry identified 6510 proteins, with 88 DEPs: 52 upregulated (*red dots*) and 36 downregulated (*blue dots*). The *gray-shaded areas* mark thresholds of $|\log_2 (\text{fold change})| \geq 0.5$ and $P < 0.05$. (**B**) The heatmap shows hierarchical clustering of iFECD and iFECD *TCF4*ΔbHLH, displaying variations in protein abundance with row *z*-scores from −2 (*blue*) to +2 (*red*). The heatmap visually splits into two distinct clusters, representing the similarity within the iFECD and iFECD *TCF4*ΔbHLH groups.

Table 1. Top 30 Upregulated Proteins in the *TCF4* Knockout Corneal Endothelial Cells Derived From the Patients With Fuchs Endothelial Corneal Dystrophy Control Subjects

Protein Name	Log_2 Fold Change	*P* Value	Gene Symbol	Entrez Gene ID
Alpha-2A adrenergic receptor	3.55	2.61×10^{-4}	ADRA2A	150
Carbonic anhydrase 2 isoform 1	2.28	1.22×10^{-6}	CA2	760
Retinal dehydrogenase 1	1.81	8.14×10^{-7}	ALDH1A1	216
Protocadherin Fat 2 isoform X1	1.61	1.64×10^{-7}	FAT2	2196
Inactive dipeptidyl peptidase 10 isoform d	1.59	1.04×10^{-4}	DPP10	57628
Prostaglandin E synthase isoform X1	1.11	3.86×10^{-4}	PTGES	9536
Lumican precursor	1.09	1.81×10^{-5}	LUM	4060
Hyaluronan and proteoglycan link protein 1 isoform X1	1.07	1.25×10^{-4}	HAPLN1	1404
Cellular retinoic acid–binding protein 2	1.02	3.85×10^{-4}	CRABP2	1382
BTB/POZ domain-containing protein KCTD12	1.01	5.45×10^{-5}	KCTD12	115207
Cystine/glutamate transporter	1.01	9.15×10^{-6}	SLC7A11	23657
Chloride intracellular channel protein 3 isoform X1	0.902	2.59×10^{-5}	CLIC3	9022
7-Methylguanosine phosphate-specific 5′-nucleotidase	0.869	2.07×10^{-4}	NT5C3B	115024
Aldose reductase isoform 1	0.868	4.13×10^{-6}	AKR1B1	231
Retinoid-binding protein 7	0.854	3.18×10^{-3}	RBP7	116362
NAD(P)H dehydrogenase [quinone] 1 isoform a	0.841	1.90×10^{-2}	NQO1	1728
4F2 cell-surface antigen heavy chain isoform b	0.829	1.76×10^{-5}	SLC3A2	6520
Spectrin beta chain, nonerythrocytic 2 isoform X1	0.820	9.93×10^{-5}	SPTBN2	6712
Zinc finger protein Rlf	0.778	4.36×10^{-2}	RLF	6018
Rho-related GTP-binding protein RhoB precursor	0.769	1.44×10^{-5}	RHOB	388
Aldo-keto reductase family 1 member B10	0.760	2.80×10^{-4}	AKR1B10	57016
Argininosuccinate synthase isoform X1	0.733	3.73×10^{-4}	ASS1	445
Protein CYR61 precursor	0.725	2.36×10^{-3}	CYR61	3491
Large neutral amino acids transporter small subunit 1	0.715	9.62×10^{-5}	SLC7A5	8140
Pituitary tumor-transforming gene 1 protein-interacting protein isoform 1 precursor	0.694	1.05×10^{-2}	PTTG1IP	754
Band 4.1-like protein 1 isoform X9	0.682	4.78×10^{-2}	EPB41L1	2036
Sulfate transporter isoform X1	0.645	4.54×10^{-4}	SLC26A2	1836
Retrotransposon-derived protein PEG10 isoform 3	0.639	6.77×10^{-4}	PEG10	23089
Phospholipid phosphatase 3	0.637	3.51×10^{-4}	PLPP3	8613
Annexin A8–like protein 1 isoform 1	0.632	354×10^{-3}	ANXA8L1	728113

Investigative Ophthalmology & Visual Science

Table 2. Top 30 Downregulated Proteins in the *TCF4* Knockout Corneal Endothelial Cells Derived From the Patients With Fuchs Endothelial Corneal Dystrophy Control Subjects

Protein Name	Log_2 Fold Change	*P* Value	Gene Symbol	Entrez Gene ID
Keratin, type I cytoskeletal 19	−1.59	6.45×10^{-4}	KRT19	3880
Calponin-1 isoform 1	−1.17	3.84×10^{-4}	CNN1	1264
Contactin-associated protein 1 precursor	−0.879	2.25×10^{-5}	CNTNAP1	8506
Epiplakin isoform X3	−0.843	1.45×10^{-3}	EPPK1	83481
Syndecan-1 isoform X1	−0.834	1.19×10^{-2}	SDC1	6382
Filamin-B isoform 2	−0.827	1.34×10^{-2}	FLNB	2317
NADH-cytochrome b5 reductase 2 isoform X1	−0.812	2.98×10^{-5}	CYB5R2	51700
Tropomyosin alpha-1 chain isoform Tpm1.6cy	−0.800	3.78×10^{-2}	TPM1	7168
Centrosomal protein of 97 kDa isoform 1	−0.796	1.29×10^{-2}	CEP97	79598
MANSC domain-containing protein 1 isoform 1 precursor	−0.788	5.95×10^{-3}	MANSC1	54682
Collagen alpha-2 (I) chain precursor	−0.748	3.73×10^{-6}	COL1A2	1278
Creatine kinase B–type isoform 2	−0.741	1.22×10^{-3}	CKB	1152
Rho GDP-dissociation inhibitor 2 isoform X1	−0.715	3.90×10^{-4}	ARHGDIB	397
Pyruvate kinase PKM isoform c	−0.673	3.93×10^{-3}	PKM	5315
Telomerase reverse transcriptase isoform 1	−0.664	2.80×10^{-2}	TERT	7015
DNA-binding protein RFXANK isoform a	−0.657	8.35×10^{-3}	RFXANK	8625
Nuclear receptor coactivator 7 isoform X1	−0.648	6.76×10^{-4}	NCOA7	135112
Protein ECT2 isoform X1	−0.645	1.72×10^{-2}	ECT2	1894
Lathosterol oxidase	−0.641	5.13×10^{-3}	SC5D	6309
Adipogenesis regulatory factor	−0.636	4.77×10^{-2}	ADIRF	10974
Extracellular sulfatase Sulf-1 isoform X1	−0.619	5.94×10^{-6}	SULF1	23213
Caspase-1 isoform alpha precursor	−0.616	8.64×10^{-3}	CASP1	834
Alpha-crystallin B chain isoform 1	−0.605	1.29×10^{-4}	CRYAB	1410
GTP cyclohydrolase 1 feedback regulatory protein	−0.597	5.23×10^{-5}	GCHFR	2644
Fructose-1,6-bisphosphatase isozyme 2	−0.587	6.16×10^{-3}	FBP2	8789
Centrosomal protein of 164 kDa isoform X6	−0.586	2.90×10^{-2}	CEP164	22897
Collagen alpha-1 (VIII) chain precursor	−0.585	4.64×10^{-2}	COL8A1	1295
Serine/threonine-protein kinase 26 isoform 1	−0.580	2.79×10^{-5}	STK26	51765
Aryl hydrocarbon receptor	−0.572	2.73×10^{-3}	AHR	196
Myelin expression factor 2 isoform a	−0.568	2.24×10^{-4}	MYEF2	50804

ern blotting showed that TGF-β2 induced the cleavage of caspase-3 and PARP in iFECD. Conversely, the TGF-β2–mediated cleavages of caspase-3 and PARP were reduced in iFECD *TCF4*$^{-/-}$ and iFECD *TCF4*ΔbHLH (Fig. 6C). Flow cytometric analysis showed that TGF-β2 treatment increased the percentage of Annexin V–positive cells to 31.4% ± 2.0% in iFECD. The percentage of Annexin V–positive cells in TGF-β2–treated iFECD TCF4$^{-/-}$ cells showed a trend toward reduction (19.8% ± 1.3%), although this difference did not reach statistical significance ($P = 5.28 \times 10^{-2}$). In contrast, TGF-β2–treated iFECD *TCF4*ΔbHLH cells exhibited a significant decrease in Annexin V–positive cells (18.0% ± 1.6%, $P = 3.02 \times 10^{-2}$) compared to TGF-β2–treated iFECD cells (Fig. 6D). Representative flow cytometric dot plots illustrating the gating parameters for all experimental conditions are presented in Supplementary Figure S2.

Western blotting confirmed the suppression of *TCF4* in iFECD *TCF4*$^{-/-}$. In terms of molecules related to the EMT, Snail1 was upregulated in iFECD by TGF-β2, but this TGF-β2–mediated upregulation of Snail1 was suppressed in both iFECD *TCF4*$^{-/-}$ and iFECD *TCF4*ΔbHLH. ZEB1 was not altered by TGF-β2 in any of the cell lines. The expression level of fibronectin was increased by TGF-β2 in iFECD but not in either iFECD *TCF4*$^{-/-}$ or iFECD *TCF4*ΔbHLH (Fig. 6E). Phosphorylation of Smad2 and Smad3 by TGF-β2 was observed in iFECD and iFECD *TCF4*$^{-/-}$, while it was suppressed in iFECD *TCF4*ΔbHLH (Fig. 6F). This differential response in Smad signaling suggests that the mechanism by which *TCF4* deletion rescues cells from apoptosis might involve distinct pathways in the two mutant cell lines. Quantitative analysis of these Western blot results and statistical testing are shown in Supplementary Figures S3, S4, and S5. Immunofluorescent staining showed that TGF-β2 increased fibronectin expression in iFECD but caused a smaller increase in iFECD *TCF4*$^{-/-}$. Aggresome staining showed that TGF-β2 induced unfolded proteins that partially colocalized with fibronectin. By contrast, TGF-β2 did not induce unfolded proteins in iFECD *TCF4*$^{-/-}$ (Fig. 7A). Quantitative analysis of colocalization using Manders's coefficient showed significantly higher coefficient in TGF-β2–treated iFECD (0.735 ± 0.040) compared to TGF-β2–treated iFECD *TCF4*$^{-/-}$ (0.152 ± 0.014, $P = 1.41 \times 10^{-3}$) (Fig. 7B).

Discussion

The aim of this study was to elucidate the role of *TCF4* in FECD pathophysiology by conducting a proteomic analysis of the FECD cell model after CRISPR/Cas9 knockout of *TCF4*. This manipulation enabled the identification of DEPs and pathways for understanding the molecular mechanisms underlying FECD. Liquid chromatography–MS analysis followed by pathway enrichment analysis identified significant molecular pathways potentially involved in the pathogenesis of FECD.

TCF4, a bHLH family member, is located on chromosome 18q21.2 (OMIM #602272; ENSG00000196628). *TCF4* regulates gene expression by binding to E-box DNA sequences,

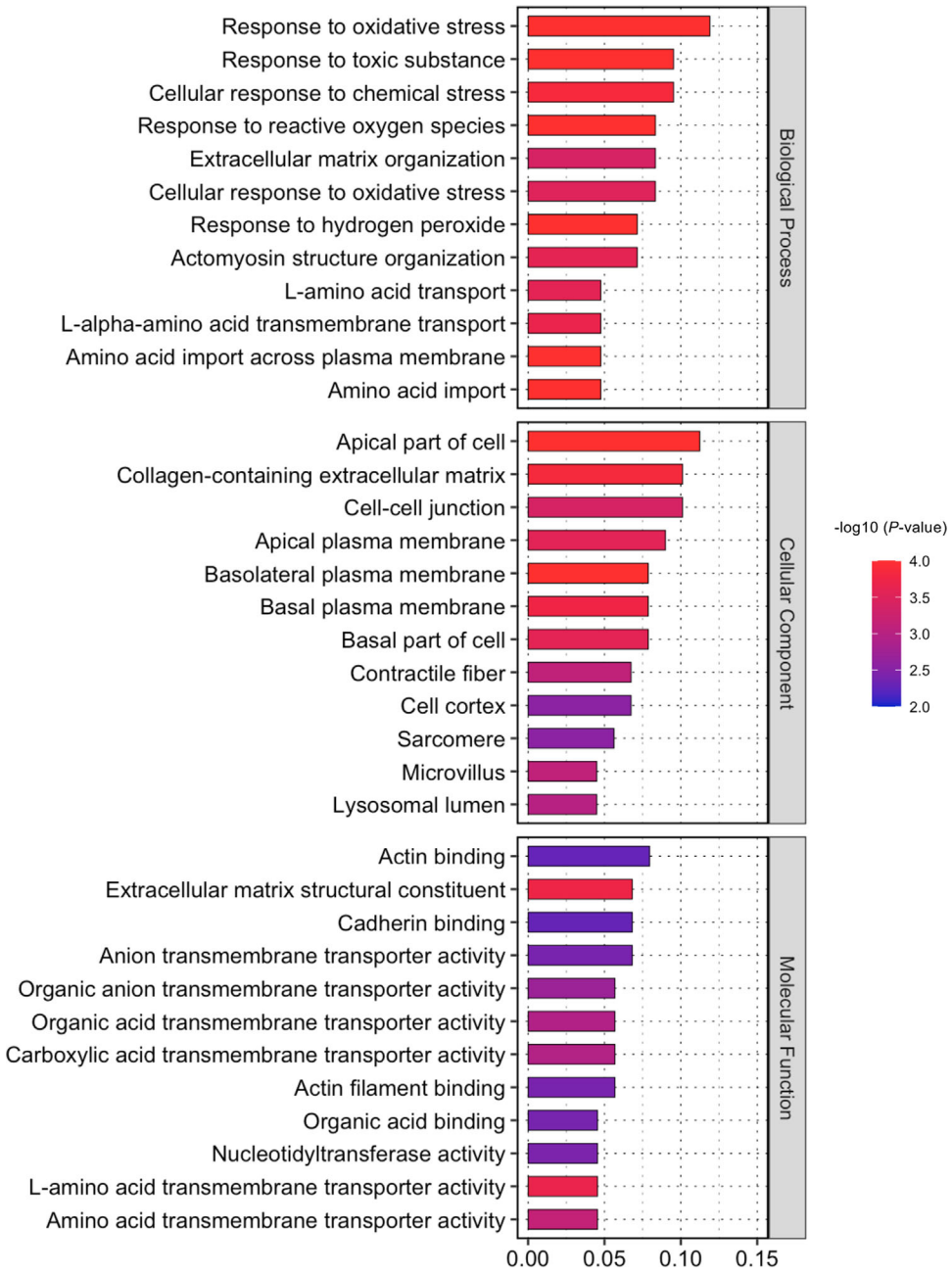

Figure 3. GO analysis of DEPs between FECD cell model (iFECD) and iFECD *TCF4*ΔbHLH. GO analysis was performed on the 88 DEPs associated with *TCF4* deletion. Significantly enriched GO terms were identified with a *P* value threshold of <0.05. The GO terms are categorized into three groups: BP, CC, and MF. In BP, significant enrichments include response to oxidative stress, response to toxic substance, and cellular response to chemical stress. In CC, enrichments include the apical part of the cell, collagen-containing ECM, and cell–cell junction. In MF, significant enrichments include actin binding, ECM structural constituent, and cadherin binding.

thereby influencing a broad spectrum of developmental and cellular processes. However, the role of *TCF4* varies depending on the cell type and disease. Numerous studies have linked *TCF4* to various neurodevelopmental disorders, with common genetic variants now associated with increased susceptibility to schizophrenia[58–60] and primary sclerosing cholangitis.[61,62] Rare mutations in *TCF4* are causes of Pitt–Hopkins syndrome, a condition characterized by intellectual disability and developmental delays.[63–67] The critical role of *TCF4* in neurodevelopment is substantiated by knockout mouse models, which exhibit significant neurodevelopmental defects and abnormal neuronal migration.[68] These findings underscore the importance of *TCF4* in normal brain development and function. In the immune system, *TCF4* is essential for the development of plasmacytoid dendritic cells, which play a crucial role in antiviral responses.[69,70] *TCF4* is also involved in the EMT, a process vital for embryonic development, tissue repair, and cancer metastasis in epithelial cells of the kidney and neuroblastoma cells.[71–75] In FECD, the discovery that a major portion of patients with FECD harbor a trinucleotide repeat expansion in *TCF4* has led to significant research efforts directed toward under-

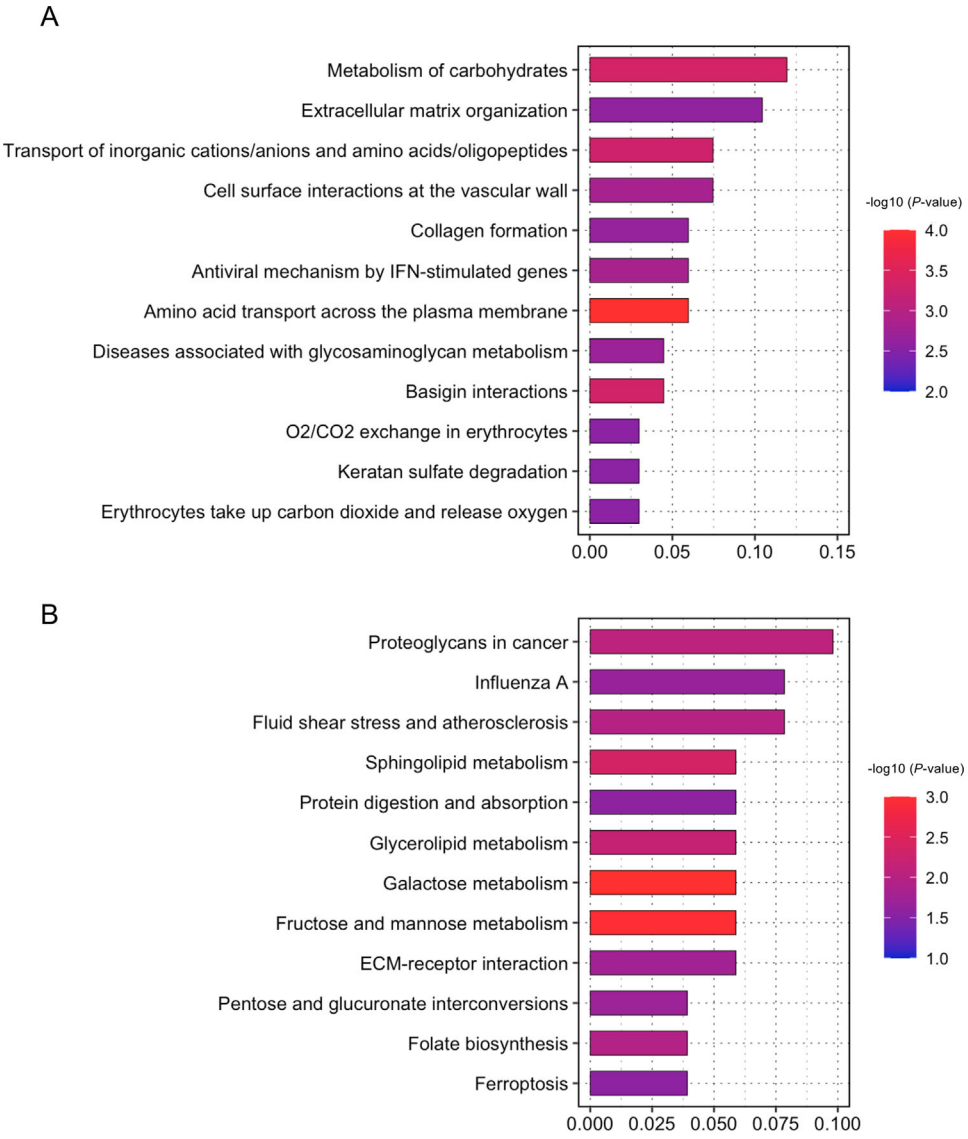

Figure 4. Enrichment analyses of DEPs between FECD cell model (iFECD) and iFECD *TCF4*ΔbHLH. (**A**) Reactome pathway analysis showed DEPs enriched in carbohydrate metabolism, ECM organization, transport of inorganic cations/anions and amino acids/oligopeptides, cell surface interactions at the vascular wall, and collagen formation. (**B**) KEGG pathway analysis demonstrated enrichment in proteoglycans in cancer, sphingolipid metabolism, protein digestion and absorption, ECM–receptor interaction, and ferroptosis.

standing how *TCF4* contributes to the pathogenesis of FECD.[23]

Various mechanisms have been proposed to elucidate how the repeat expansion in *TCF4* impacts cellular functions in FECD. A primary hypothesis is that *TCF4* is dysregulated because the repeat expansion alters expression levels and splicing of *TCF4* transcripts.[27,33–38,76] This disruption can lead to aberrant splicing and dysregulated expression of specific *TCF4* isoforms, thereby disrupting normal cellular functions.[34,37,39] Another proposed mechanism is RNA-mediated toxicity, as the expanded repeat RNA transcripts sequester RNA-binding proteins, such as muscleblind-like (MBNL) proteins, leading to widespread splicing dysregulation. This process mirrors the pathogenic mechanism seen in myotonic dystrophy, another trinucleotide repeat disorder.[77–79] In FECD, the sequestration of MBNL proteins by expanded repeats in *TCF4* RNA results in abnormal splicing of multiple genes, contributing to cellular dysfunction.[24,28,80,81] Repeat-associated non-AUG translation[82] has also been identified as a potential pathogenic mechanism.[29] This process produces toxic polypeptides from expanded-repeat RNA without a traditional start codon. These peptides can aggregate, disrupting cellular homeostasis and inducing cell death. However, despite these significant advancements in understanding the role of *TCF4* in FECD, many aspects of the disease mechanism remain elusive, including the exact role of *TCF4* in the corneal endothelium.[23]

Previous studies mainly studied the transcriptome by analyzing samples obtained from FECD with repeat expansion in *TCF4*, FECD without repeat expansion, and non-FECD subjects. The limited availability of clinical samples of corneal endothelium has hampered a comprehensive proteome analysis. However, proteomics is an indispensable addition to transcriptome analysis because it captures the dynamic and functional aspects of proteins that are not reflected at the RNA level.[40–43] The current pathway

Investigative Ophthalmology & Visual Science

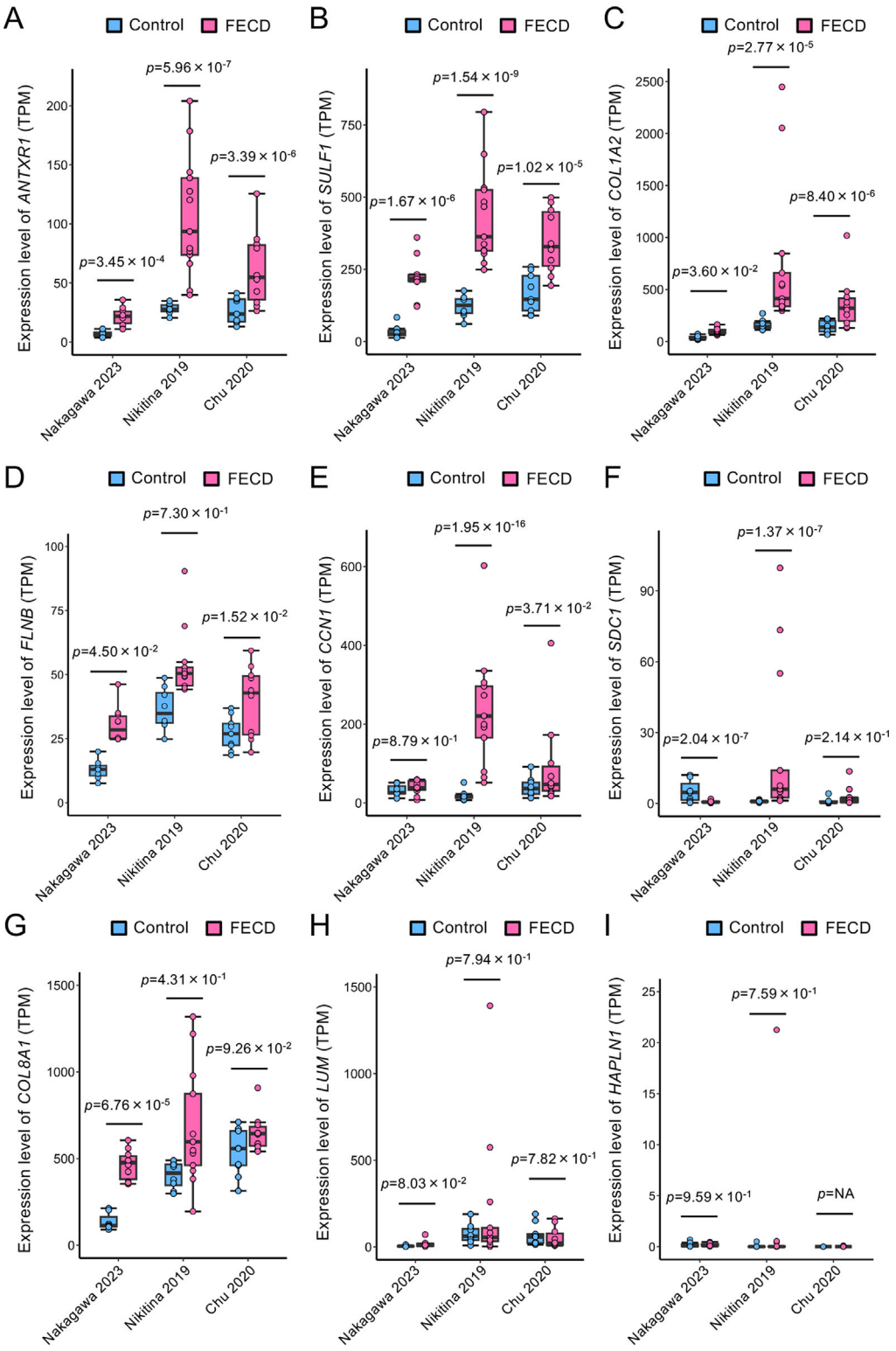

Figure 5. Confirmation of altered ECM molecules at the mRNA level using RNA-seq data. Expression levels of ECM-related mRNAs corresponding to DEPs were analyzed using three previously published RNA-seq data sets, including our own.[38,50,51] *ANTXR1* (**A**), *SULF1* (**B**), and *COL1A2* (**C**) show consistent upregulation across all data sets in corneal endothelial cells from patients with FECD compared to controls. *FLNB* (**D**) was upregulated in Nakagawa et al.[38] and Chu et al.,[50] while *CCN1* (**E**) showed increased expression in Nikitina et al.[51] and Chu et al.[50] *SDC1* (**F**) exhibited decreased expression in Nakagawa et al.[38] but increased expression in Nikitina et al.[51] *COL8A1* (**G**) showed upregulation only in Nakagawa et al.[38] *LUM* (**H**) and *HAPLN1* (**I**) showed no significant changes in any data set.

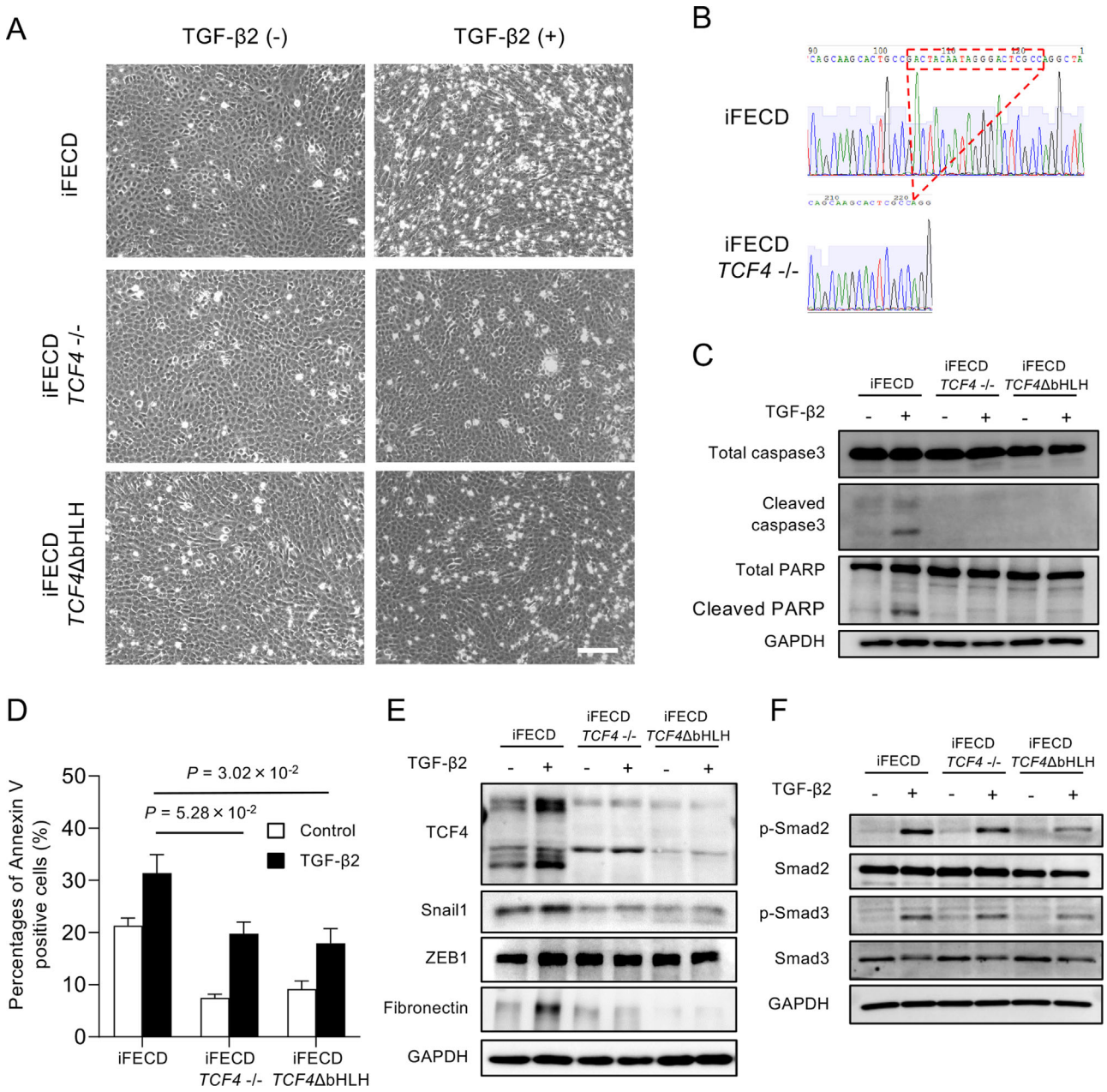

Figure 6. Effect of *TCF4* knockout on TGF-β2–mediated ECM production and apoptosis. (**A**) The bHLH region or 20 bases in exon 9 of *TCF4* in iFECD were knocked out using CRISPR/Cas9 (iFECD *TCF4*$^{-/-}$, iFECD *TCF4*ΔbHLH). Cells were cultured in serum-free medium for 24 hours, then treated with or without TGF-β2 (10 ng/mL) for 24 hours. Phase-contrast images show that iFECD forms a monolayer with polygonal morphology. TGF-β2–induced cell death in iFECD but not in iFECD *TCF4*$^{-/-}$ or iFECD *TCF4*ΔbHLH. *Scale bar*: 200 µm. (**B**) Sanger sequencing confirmed the deletion of 20 bases in exon 9 of *TCF4* in iFECD *TCF4*$^{-/-}$. *Red lines* indicate the deleted bases. (**C**) Western blotting showed TGF-β2–induced cleavage of caspase-3 and PARP in iFECD, which was suppressed in iFECD *TCF4*$^{-/-}$ and iFECD *TCF4*ΔbHLH. (**D**) Flow cytometric analysis of Annexin V–positive apoptotic cells in response to TGF-β2 treatment. TGF-β2 treatment substantially increased the percentage of Annexin V–positive cells to 31.4% ± 2.0% in iFECD cells. Both iFECD *TCF4*$^{-/-}$ and iFECD *TCF4*ΔbHLH cells demonstrated resistance to TGF-β2–induced apoptosis, showing lower percentages of Annexin V–positive cells (19.8% ± 1.3% and 18.0% ± 1.6%, respectively; $P = 5.28 \times 10^{-2}$ and $P = 3.02 \times 10^{-2}$, compared to TGF-β2–treated iFECD). Data are presented as mean ± SEM from three independent experiments. (**E**) Western blotting confirmed suppression of TCF4 in both iFECD *TCF4*$^{-/-}$ and iFECD *TCF4*ΔbHLH. TGF-β2 upregulated Snail1 in iFECD, but this upregulation was suppressed in both mutant cell lines. ZEB1 expression was unaffected by TGF-β2 in all cell lines. Fibronectin levels increased in iFECD but not in either iFECD *TCF4*$^{-/-}$ or iFECD *TCF4*ΔbHLH with TGF-β2 treatment. (**F**) Phosphorylation of Smad2 and Smad3 by TGF-β2 was confirmed in both iFECD and iFECD *TCF4*$^{-/-}$, while this phosphorylation was suppressed in iFECD *TCF4*ΔbHLH. All experiments were performed independently at least three times with reproducible results.

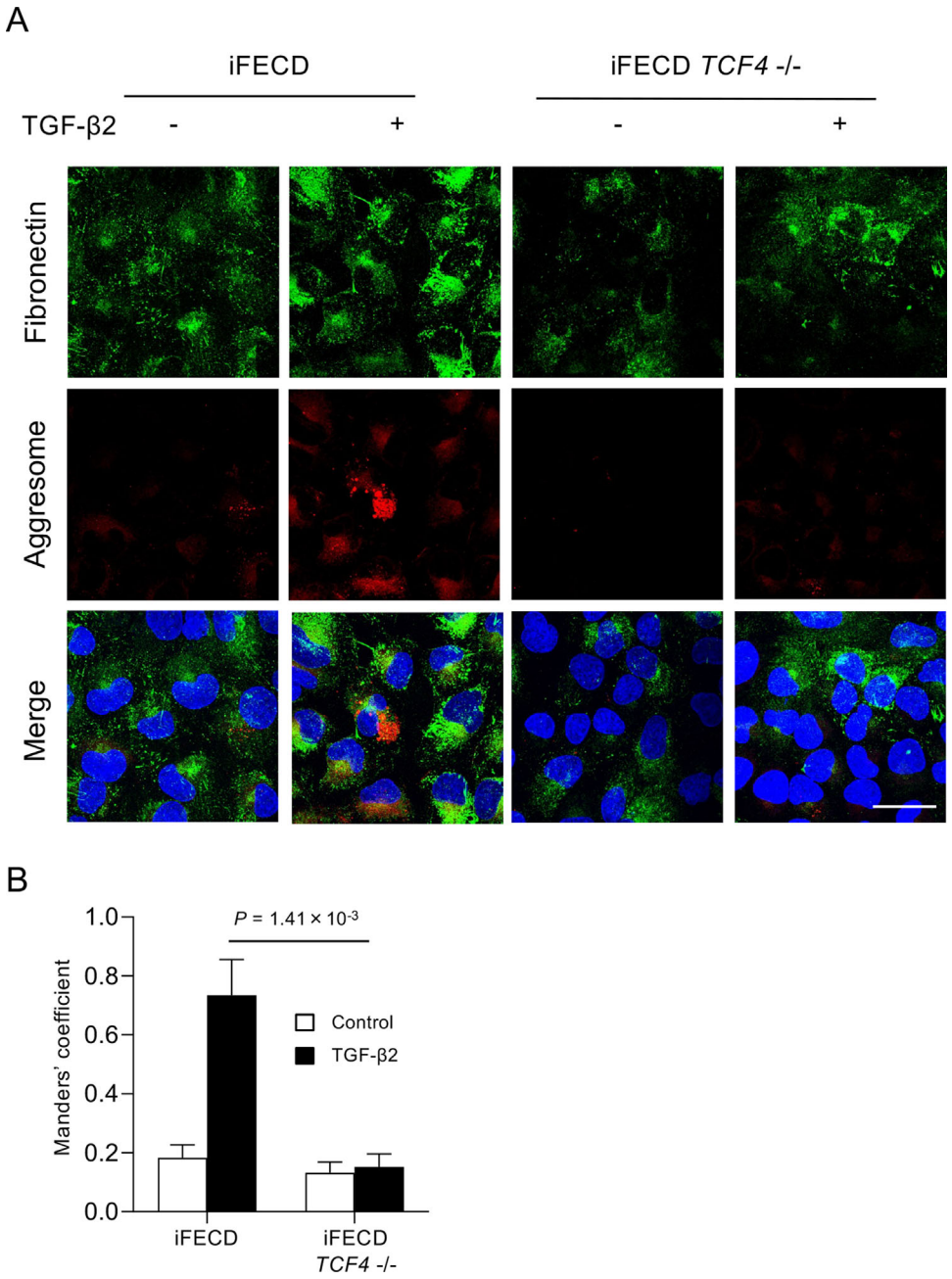

Figure 7. Effect of *TCF4* knockout on TGF-β2 mediated unfolded protein deposition. (**A**) iFECD and iFECD *TCF4*$^{-/-}$ cells were cultured with or without TGF-β2 (10 ng/mL) for 24 hours. Fibronectin production and unfolded protein deposition were evaluated by immunofluorescent staining and aggresome staining, respectively. Immunofluorescent staining showed that TGF-β2 increased fibronectin expression in iFECD but showed a lesser increase in iFECD *TCF4*$^{-/-}$. Aggresome staining indicated that TGF-β2 induced unfolded protein partially colocalizing with fibronectin in iFECD. In contrast, TGF-β2 did not induce unfolded protein in iFECD *TCF4*$^{-/-}$. To ensure reproducibility, all experiments were performed in triplicate ($n = 3$ independent experiments), yielding similar results. Representative images are presented. *Scale bar*: 50 µm. (**B**) Colocalization between aggresome and fibronectin signals was quantified using Manders's coefficient. Values are expressed as mean ± SEM from three independent experiments.

analyses at the protein level revealed that multiple ECM-related pathways are associated with *TCF4*. The guttae induced by excessive deposition of ECM components[83,84] are diagnostic FECD features, and they are responsible for reduced visual function due to light scattering.[85,86] Our proteome analyses presented here have added evidence that *TCF4* plays a pivotal role in the phenotypic features of FECD.

In FECD, corneal endothelial cells lose their epithelial cell phenotype and transform into a mesenchymal phenotype associated with the production of multiple ECM components; some researchers have proposed that this process is the EMT or endothelial–mesenchymal transition.[30,46,87] The EMT is a crucial process in development, wound healing, and pathologic conditions like fibrosis and cancer metastasis.[88] Our current data support an involvement of *TCF4*

in the EMT in corneal endothelial cells, although further study using multiple EMT markers is necessary. We previously reported that excessive production of ECM proteins, including fibronectin and collagen type 1, results in the formation of unfolded proteins in the corneal endothelium, as observed in samples obtained from patients with FECD.[56,57] Our previous in vitro study using the FECD cell model showed that TGF-β, which plays a pivotal role in EMT by activating intracellular signaling pathways, such as the Smad and non-Smad pathways, increases the production of ECM, resulting in apoptosis mediated by the unfolded protein response.[56,57] In the current study, the deletion of *TCF4* suppressed this formation of unfolded protein and counteracted TGF-β–mediated apoptosis of the FECD cell model. These results suggest that *TCF4* induces the EMT and causes excessive production of pathologic ECM molecules, which eventually cause endoplasmic reticulum stress–induced apoptosis.

The remaining question is how *TCF4* induces pathologic processes only in patients with FECD but not in healthy subjects. We recently analyzed three RNA-seq data sets for corneal endothelial cells derived from non-FECD and FECD subjects. We found that one isoform of *TCF4*, among at least 93 isoforms, was upregulated in the corneal endothelium of patients with FECD harboring repeat expansion in *TCF4*. The discovery of this isoform, *TCF4-277* (ENST00000636400.2), indicated that a dysregulated isoform of *TCF4* associated with repeat expansion potentially induces the pathologic process of FECD.[38,89] Our current results indicate that deletion of *TCF4* in the FECD cell model suppresses the disease phenotype, providing further support for the concept that dysregulated *TCF4* plays an important role in pathophysiology.

One limitation of the present study is the lack of FECD cells without repeat expansion; therefore, the precise role of *TCF4* in FECD without expansion is still unclear. Similar analyses using corneal endothelial cells derived from multiple patients with FECD are also necessary, as the severity of FECD varies widely depending on the individual. In summary, our present findings highlight the critical role of *TCF4* in the pathophysiology of FECD, particularly implicating ECM-related pathways and TGF-β–mediated cell death. Further investigation of the role of dysregulated *TCF4* might reveal the precise details of FECD pathophysiology and provide potential therapy targeting *TCF4* or associated pathways.

Acknowledgments

Supported by JSPS KAKENHI Grant 18K09464 to NO and by SERB, Government of India (EMR/2015/000607), to SVE.

Disclosure: **T. Nakagawa**, None; **T. Honda**, None; **T. Yuasa**, None; **G. Nishiuchi**, None; **M. Sato**, None; **A. Tokunaga**, None; **M. Nakahara**, None; **T. Tourtas**, None; **U. Schlötzer-Schrehardt**, None; **F. Kruse**, None; **P. Padmanabhan**, None; **A. Chatterjee**, None; **G. Sathe**, None; **V. Ghose**, None; **N. Janakiraman**, None; **D.J. Blake**, None; **N. Koizumi**, None; **S. Elchuri**, None; **N. Okumura**, None

References

1. Eghrari AO, Riazuddin SA, Gottsch JD. Fuchs corneal dystrophy. *Prog Mol Biol Transl Sci*. 2015;134:79–97.
2. Ong Tone S, Kocaba V, Bohm M, Wylegala A, White TL, Jurkunas UV. Fuchs endothelial corneal dystrophy: the vicious cycle of Fuchs pathogenesis. *Prog Retin Eye Res*. 2021;80:100863.
3. Krachmer JH, Purcell JJ, Jr, Young CW, Bucher KD. Corneal endothelial dystrophy. A study of 64 families. *Arch Ophthalmol*. 1978;96:2036–2039.
4. Kitagawa K, Kojima M, Sasaki H, et al. Prevalence of primary cornea guttata and morphology of corneal endothelium in aging Japanese and Singaporean subjects. *Ophthalmic Res*. 2002;34:135–138.
5. Zoega GM, Fujisawa A, Sasaki H, et al. Prevalence and risk factors for cornea guttata in the Reykjavik Eye Study. *Ophthalmology*. 2006;113:565–569.
6. Higa A, Sakai H, Sawaguchi S, et al. Prevalence of and risk factors for cornea guttata in a population-based study in a southwestern island of Japan: the Kumejima study. *Arch Ophthalmol*. 2011;129:332–336.
7. Aiello F, Gallo Afflitto G, Ceccarelli F, Cesareo M, Nucci C. Global prevalence of Fuchs endothelial corneal dystrophy (FECD) in adult population: a systematic review and meta-analysis. *J Ophthalmol*. 2022;2022:3091695.
8. Vithana EN, Morgan PE, Ramprasad V, et al. SLC4A11 mutations in Fuchs endothelial corneal dystrophy. *Hum Mol Genet*. 2008;17:656–666.
9. Riazuddin SA, Vithana EN, Seet LF, et al. Missense mutations in the sodium borate cotransporter SLC4A11 cause late-onset Fuchs corneal dystrophy. *Hum Mutat*. 2010;31:1261–1268.
10. Riazuddin SA, Parker DS, McGlumphy EJ, et al. Mutations in LOXHD1, a recessive-deafness locus, cause dominant late-onset Fuchs corneal dystrophy. *Am J Hum Genet*. 2012;90:533–539.
11. Tang H, Zhang W, Yan XM, et al. Analysis of SLC4A11, ZEB1, LOXHD1, COL8A2 and TCF4 gene sequences in a multigenerational family with late-onset Fuchs corneal dystrophy. *Int J Mol Med*. 2016;37:1487–1500.
12. Rao BS, Ansar S, Arokiasamy T, et al. Analysis of candidate genes ZEB1 and LOXHD1 in late-onset Fuchs' endothelial corneal dystrophy in an Indian cohort. *Ophthalmic Genet*. 2018;39:443–449.
13. Riazuddin SA, Vasanth S, Katsanis N, Gottsch JD. Mutations in AGBL1 cause dominant late-onset Fuchs corneal dystrophy and alter protein-protein interaction with TCF4. *Am J Hum Genet*. 2013;93:758–764.
14. Afshari NA, Igo RP, Jr, Morris NJ, et al. Genome-wide association study identifies three novel loci in Fuchs endothelial corneal dystrophy. *Nat Commun*. 2017;8:14898.
15. Okumura N, Hayashi R, Nakano M, et al. Association of rs613872 and trinucleotide repeat expansion in the TCF4 gene of German patients with Fuchs endothelial corneal dystrophy. *Cornea*. 2019;38:799–805.
16. Wieben ED, Aleff RA, Tosakulwong N, et al. A common trinucleotide repeat expansion within the transcription factor 4 (TCF4, E2-2) gene predicts Fuchs corneal dystrophy. *PloS one*. 2012;7:e49083.
17. Mootha VV, Gong X, Ku HC, Xing C. Association and familial segregation of CTG18.1 trinucleotide repeat expansion of TCF4 gene in Fuchs' endothelial corneal dystrophy. *Invest Ophthalmol Vis Sci*. 2014;55:33–42.
18. Nanda GG, Padhy B, Samal S, Das S, Alone DP. Genetic association of TCF4 intronic polymorphisms, CTG18.1 and rs17089887, with Fuchs' endothelial corneal dystrophy in an Indian population. *Invest Ophthalmol Vis Sci*. 2014;55:7674–7680.
19. Mootha VV, Hussain I, Cunnusamy K, et al. TCF4 triplet repeat expansion and nuclear RNA foci in Fuchs' endothelial corneal dystrophy. *Invest Ophthalmol Vis Sci*. 2015;56:2003–2011.

20. Nakano M, Okumura N, Nakagawa H, et al. Trinucleotide repeat expansion in the TCF4 gene in Fuchs' endothelial corneal dystrophy in Japanese. *Invest Ophthalmol Vis Sci*. 2015;56:4865–4869.
21. Eghrari AO, Vahedi S, Afshari NA, Riazuddin SA, Gottsch JD. CTG18.1 Expansion in TCF4 among African Americans with Fuchs' corneal dystrophy. *Invest Ophthalmol Vis Sci*. 2017;58:6046–6049.
22. Okumura N, Puangsricharern V, Jindasak R, et al. Trinucleotide repeat expansion in the transcription factor 4 (TCF4) gene in Thai patients with Fuchs endothelial corneal dystrophy. *Eye (Lond)*. 2020;34:880–885.
23. Fautsch MP, Wieben ED, Baratz KH, et al. TCF4-mediated Fuchs endothelial corneal dystrophy: Insights into a common trinucleotide repeat-associated disease. *Prog Retin Eye Res*. 2021;81:100883.
24. Du J, Aleff RA, Soragni E, et al. RNA toxicity and missplicing in the common eye disease Fuchs endothelial corneal dystrophy. *J Biol Chem*. 2015;290:5979–5990.
25. Soliman AZ, Xing C, Radwan SH, Gong X, Mootha VV. Correlation of severity of Fuchs endothelial corneal dystrophy with triplet repeat expansion in TCF4. *JAMA Ophthalmol*. 2015;133:1386–1391.
26. Kuot A, Hewitt AW, Snibson GR, et al. TGC repeat expansion in the TCF4 gene increases the risk of Fuchs' endothelial corneal dystrophy in Australian cases. *PLoS One*. 2017;12:e0183719.
27. Foja S, Luther M, Hoffmann K, Rupprecht A, Gruenauer-Kloevekorn C. CTG18.1 repeat expansion may reduce TCF4 gene expression in corneal endothelial cells of German patients with Fuchs' dystrophy. *Graefes Arch Clin Exp Ophthalmol*. 2017;255:1621–1631.
28. Hu J, Rong Z, Gong X, et al. Oligonucleotides targeting TCF4 triplet repeat expansion inhibit RNA foci and missplicing in Fuchs' dystrophy. *Hum Mol Genet*. 2018;27:1015–1026.
29. Soragni E, Petrosyan L, Rinkoski TA, et al. Repeat-associated non-ATG (RAN) translation in Fuchs' endothelial corneal dystrophy. *Invest Ophthalmol Vis Sci*. 2018;59:1888–1896.
30. Okumura N, Minamiyama R, Ho LT, et al. Involvement of ZEB1 and Snail1 in excessive production of extracellular matrix in Fuchs endothelial corneal dystrophy. *Lab Invest*. 2015;95:1291–1304.
31. Matthaei M, Gillessen J, Muether PS, et al. Epithelial-mesenchymal transition (EMT)-related cytokines in the aqueous humor of phakic and pseudophakic Fuchs' dystrophy eyes. *Invest Ophthalmol Vis Sci*. 2015;56:2749–2754.
32. Katikireddy KR, White TL, Miyajima T, et al. NQO1 downregulation potentiates menadione-induced endothelial-mesenchymal transition during rosette formation in Fuchs endothelial corneal dystrophy. *Free Radic Biol Med*. 2018;116:19–30.
33. Wieben ED, Aleff RA, Eckloff BW, et al. Comprehensive assessment of genetic variants within TCF4 in Fuchs' endothelial corneal dystrophy. *Invest Ophthalmol Vis Sci*. 2014;55:6101–6107.
34. Wieben ED, Aleff RA, Tang X, et al. Trinucleotide repeat expansion in the transcription factor 4 (TCF4) gene leads to widespread mRNA splicing changes in Fuchs' endothelial corneal dystrophy. *Invest Ophthalmol Vis Sci*. 2017;58:343–352.
35. Wieben ED, Aleff RA, Tang X, et al. Gene expression in the corneal endothelium of Fuchs endothelial corneal dystrophy patients with and without expansion of a trinucleotide repeat in TCF4. *PLoS One*. 2018;13:e0200005.
36. Okumura N, Hayashi R, Nakano M, et al. Effect of trinucleotide repeat expansion on the expression of TCF4 mRNA in Fuchs' endothelial corneal dystrophy. *Invest Ophthalmol Vis Sci*. 2019;60:779–786.
37. Sirp A, Leite K, Tuvikene J, Nurm K, Sepp M, Timmusk T. The Fuchs corneal dystrophy-associated CTG repeat expansion in the TCF4 gene affects transcription from its alternative promoters. *Sci Rep*. 2020;10:18424.
38. Nakagawa T, Tokuda Y, Nakano M, et al. RNA-seq-based transcriptome analysis of corneal endothelial cells derived from patients with Fuchs endothelial corneal dystrophy. *Sci Rep*. 2023;13:8647.
39. Honda T, Nakagawa T, Yuasa T, et al. Dysregulation of the TCF4 isoform in corneal endothelial cells of patients with Fuchs endothelial corneal dystrophy. *Invest Ophthalmol Vis Sci*. 2024;65:27.
40. MacKay VL, Li X, Flory MR, et al. Gene expression analyzed by high-resolution state array analysis and quantitative proteomics: response of yeast to mating pheromone. *Mol Cell Proteomics*. 2004;3:478–489.
41. Lundberg E, Fagerberg L, Klevebring D, et al. Defining the transcriptome and proteome in three functionally different human cell lines. *Mol Syst Biol*. 2010;6:450.
42. Kumar D, Bansal G, Narang A, Basak T, Abbas T, Dash D. Integrating transcriptome and proteome profiling: strategies and applications. *Proteomics*. 2016;16:2533–2544.
43. Gutierrez Reyes CD, Alejo-Jacuinde G, Perez Sanchez B, et al. Multi omics applications in biological systems. *Curr Issues Mol Biol*. 2024;46:5777–5793.
44. Tyanova S, Temu T, Sinitcyn P, et al. The Perseus computational platform for comprehensive analysis of (prote)omics data. *Nat Methods*. 2016;13:731–740.
45. Harris MA, Clark J, Ireland A, et al. The Gene Ontology (GO) database and informatics resource. *Nucleic Acids Res*. 2004;32:D258–D261.
46. Stunf Pukl S. MicroRNA of epithelial to mesenchymal transition in Fuchs' endothelial corneal dystrophy. *Genes (Basel)*. 2022;13(10):1711.
47. Joshi-Tope G, Gillespie M, Vastrik I, et al. Reactome: a knowledgebase of biological pathways. *Nucleic Acids Res*. 2005;33:D428–D432.
48. Kanehisa M, Goto S. KEGG: Kyoto Encyclopedia of Genes and Genomes. *Nucleic Acids Res*. 2000;28:27–30.
49. Kanehisa M, Sato Y, Kawashima M, Furumichi M, Tanabe M. KEGG as a reference resource for gene and protein annotation. *Nucleic Acids Res*. 2016;44:D457–D462.
50. Chu Y, Hu J, Liang H, et al. Analyzing pre-symptomatic tissue to gain insights into the molecular and mechanistic origins of late-onset degenerative trinucleotide repeat disease. *Nucleic Acids Res*. 2020;48:6740–6758.
51. Nikitina AS, Belodedova AV, Malyugin BE, et al. Dataset on transcriptome profiling of corneal endothelium from patients with Fuchs endothelial corneal dystrophy. *Data Brief*. 2019;25:104047.
52. Chen S, Zhou Y, Chen Y, Gu J. fastp: an ultra-fast all-in-one FASTQ preprocessor. *Bioinformatics*. 2018;34:i884–i890.
53. Li B, Dewey CN. RSEM: accurate transcript quantification from RNA-seq data with or without a reference genome. *BMC Bioinformatics*. 2011;12:323.
54. Putri GH, Anders S, Pyl PT, Pimanda JE, Zanini F. Analysing high-throughput sequencing data in Python with HTSeq 2.0. *Bioinformatics*. 2022;38:2943–2945.
55. Forrest MP, Hill MJ, Kavanagh DH, Tansey KE, Waite AJ, Blake DJ. The psychiatric risk gene transcription factor 4 (TCF4) regulates neurodevelopmental pathways associated with schizophrenia, autism, and intellectual disability. *Schizophr Bull*. 2018;44:1100–1110.
56. Okumura N, Kitahara M, Okuda H, et al. Sustained activation of the unfolded protein response induces cell death in Fuchs' endothelial corneal dystrophy. *Invest Ophthalmol Vis Sci*. 2017;58:3697–3707.

Investigative Ophthalmology & Visual Science

57. Okumura N, Hashimoto K, Kitahara M, et al. Activation of TGF-β signaling induces cell death via the unfolded protein response in Fuchs endothelial corneal dystrophy. *Sci Rep*. 2017;7:6801.
58. Lennertz L, Quednow BB, Benninghoff J, Wagner M, Maier W, Mossner R. Impact of TCF4 on the genetics of schizophrenia. *Eur Arch Psychiatry Clin Neurosci*. 2011;261(suppl 2):S161–S165.
59. Navarrete K, Pedroso I, De Jong S, et al. TCF4 (e2-2; ITF2): a schizophrenia-associated gene with pleiotropic effects on human disease. *Am J Med Genet B Neuropsychiatr Genet*. 2013;162:1–16.
60. Quednow BB, Brzozka MM, Rossner MJ. Transcription factor 4 (TCF4) and schizophrenia: integrating the animal and the human perspective. *Cell Mol Life Sci*. 2014;71:2815–2835.
61. Ellinghaus D, Folseraas T, Holm K, et al. Genome-wide association analysis in primary sclerosing cholangitis and ulcerative colitis identifies risk loci at GPR35 and TCF4. *Hepatology*. 2013;58:1074–1083.
62. Liu JZ, Hov JR, Folseraas T, et al. Dense genotyping of immune-related disease regions identifies nine new risk loci for primary sclerosing cholangitis. *Nat Genet*. 2013;45:670–675.
63. Amiel J, Rio M, de Pontual L, et al. Mutations in TCF4, encoding a class I basic helix-loop-helix transcription factor, are responsible for Pitt-Hopkins syndrome, a severe epileptic encephalopathy associated with autonomic dysfunction. *Am J Hum Genet*. 2007;80:988–993.
64. Zweier C, Peippo MM, Hoyer J, et al. Haploinsufficiency of TCF4 causes syndromal mental retardation with intermittent hyperventilation (Pitt-Hopkins syndrome). *Am J Hum Genet*. 2007;80:994–1001.
65. Sweatt JD. Pitt-Hopkins syndrome: intellectual disability due to loss of TCF4-regulated gene transcription. *Exp Mol Med*. 2013;45:e21.
66. Chen HY, Bohlen JF, Maher BJ. Molecular and cellular function of transcription factor 4 in Pitt-Hopkins syndrome. *Dev Neurosci*. 2021;43:159–167.
67. Martinowich K, Das D, Sripathy SR, Mai Y, Kenney RF, Maher BJ. Evaluation of Na(v)1.8 as a therapeutic target for Pitt Hopkins syndrome. *Mol Psychiatry*. 2023;28:76–82.
68. Flora A, Garcia JJ, Thaller C, Zoghbi HY. The E-protein Tcf4 interacts with Math1 to regulate differentiation of a specific subset of neuronal progenitors. *Proc Natl Acad Sci USA*. 2007;104:15382–15387.
69. Cisse B, Caton ML, Lehner M, et al. Transcription factor E2-2 is an essential and specific regulator of plasmacytoid dendritic cell development. *Cell*. 2008;135:37–48.
70. Ghosh HS, Cisse B, Bunin A, Lewis KL, Reizis B. Continuous expression of the transcription factor e2-2 maintains the cell fate of mature plasmacytoid dendritic cells. *Immunity*. 2010;33:905–916.
71. Sobrado VR, Moreno-Bueno G, Cubillo E, et al. The class I bHLH factors E2-2A and E2-2B regulate EMT. *J Cell Sci*. 2009;122:1014–1024.
72. Forrest MP, Waite AJ, Martin-Rendon E, Blake DJ. Knockdown of human TCF4 affects multiple signaling pathways involved in cell survival, epithelial to mesenchymal transition and neuronal differentiation. *PLoS One*. 2013;8:e73169.
73. Jiang X, Ding W, Shen W, Jin J. H19/miR-152-3p/TCF4 axis increases chemosensitivity of gastric cancer cells through suppression of epithelial-mesenchymal transition. *Transl Cancer Res*. 2020;9:3915–3925.
74. Zhang C, Wei S, Sun WP, et al. Super-enhancer-driven AJUBA is activated by TCF4 and involved in epithelial-mesenchymal transition in the progression of hepatocellular carcinoma. *Theranostics*. 2020;10:9066–9082.
75. Addison JB, Voronkova MA, Fugett JH, et al. Functional hierarchy and cooperation of EMT master transcription factors in breast cancer metastasis. *Mol Cancer Res*. 2021;19:784–798.
76. Oldak M, Ruszkowska E, Udziela M, et al. Fuchs endothelial corneal dystrophy: strong association with rs613872 not paralleled by changes in corneal endothelial TCF4 mRNA level. *Biomed Res Int*. 2015;2015:640234.
77. Kuyumcu-Martinez NM, Wang GS, Cooper TA. Increased steady-state levels of CUGBP1 in myotonic dystrophy 1 are due to PKC-mediated hyperphosphorylation. *Mol Cell*. 2007;28:68–78.
78. Sznajder LJ, Swanson MS. Short tandem repeat expansions and RNA-mediated pathogenesis in myotonic dystrophy. *Int J Mol Sci*. 2019;20(13):3365.
79. Winkler NS, Milone M, Martinez-Thompson JM, et al. Fuchs' endothelial corneal dystrophy in patients with myotonic dystrophy, type 1. *Invest Ophthalmol Vis Sci*. 2018;59:3053–3057.
80. Zarouchlioti C, Sanchez-Pintado B, Hafford Tear NJ, et al. Antisense therapy for a common corneal dystrophy ameliorates TCF4 repeat expansion-mediated toxicity. *Am J Hum Genet*. 2018;102:528–539.
81. Rong Z, Hu J, Corey DR, Mootha VV. Quantitative studies of muscleblind proteins and their interaction with TCF4 RNA foci support involvement in the mechanism of Fuchs' dystrophy. *Invest Ophthalmol Vis Sci*. 2019;60:3980–3991.
82. Zu T, Gibbens B, Doty NS, et al. Non-ATG-initiated translation directed by microsatellite expansions. *Proc Natl Acad Sci USA*. 2011;108:260–265.
83. Gottsch JD, Zhang C, Sundin OH, Bell WR, Stark WJ, Green WR. Fuchs corneal dystrophy: aberrant collagen distribution in an L450W mutant of the COL8A2 gene. *Invest Ophthalmol Vis Sci*. 2005;46:4504–4511.
84. Nakagawa T, Okumura N, Ikegawa M, et al. Shotgun proteomics identification of proteins expressed in the Descemet's membrane of patients with Fuchs endothelial corneal dystrophy. *Sci Rep*. 2023;13:10401.
85. Watanabe S, Oie Y, Fujimoto H, et al. Relationship between corneal guttae and quality of vision in patients with mild Fuchs' endothelial corneal dystrophy. *Ophthalmology*. 2015;122:2103–2109.
86. Wacker K, McLaren JW, Amin SR, Baratz KH, Patel SV. Corneal high-order aberrations and backscatter in Fuchs' endothelial corneal dystrophy. *Ophthalmology*. 2015;122:1645–1652.
87. White TL, Deshpande N, Kumar V, Gauthier AG, Jurkunas UV. Cell cycle re-entry and arrest in G2/M phase induces senescence and fibrosis in Fuchs endothelial corneal dystrophy. *Free Radic Biol Med*. 2021;164:34–43.
88. Kalluri R. EMT: when epithelial cells decide to become mesenchymal-like cells. *J Clin Invest*. 2009;119:1417–1419.
89. Tokuda Y, Okumura N, Komori Y, et al. Transcriptome dataset of human corneal endothelium based on ribosomal RNA-depleted RNA-seq data. *Sci Data*. 2020;7:407.

Investigative Ophthalmology & Visual Science